Conformation and Self-Association of a Hybrid Peptide of Cecropin A and Melittin with Improved Antibiotic Activity

Imma Fernández, Josep Ubach, Monika Fuxreiter, José Manuel Andreu, David Andreu and Miquel Pons*

Abstract: A 15-residue hybrid peptide containing residues 1–7 from cecropin A and residues 2–9 from melittin, CA(1–7)M(2–9), is a potent antibiotic with broader activity than cecropin A, but without the cytotoxic character of melittin. The conformational behaviour of CA(1–7)M(2–9) including the formation of multimeric species in solution has been investigated by circular dichroism, ultracentrifugation, electrospray mass spectrometry, NMR and energy calculations. Addition of hexafluoroisopropanol or liposomes causes the appearance of a CD spectrum characteristic of a helical structure that changes with pH, buffer and peptide concentration. The concentration dependence is atypical, as the ellipticity at 222 nm decreases with peptide concentration and is not correlated with a corresponding decrease in helix content as measured from the NMR spectra. The presence of aggregated structures is demonstrated by ultracentrifugation and ES-MS experiments, which also provide an indication of the stoichiometry. Long-range NOEs suggest a model of aggregation with neighbouring molecules packed antiparallel. Aggregation causes very slow proton–deuterium exchange in some amide protons in the C-terminal region and provides a method for estimating a very large association constant (ca. $10^6\,M^{-1}$) as well as the stoichiometry of the aggregates. The tendency to aggregate seems to be an inherited feature from melittin and may enhance the antibiotic activity either by facilitating the incorporation of the peptide into the membrane in large quantities or by promoting the disruption of the membrane.

Keywords
aggregation · antibiotics · circular dichroism · helices · peptides

Introduction

Antibacterial peptides are an important component of the defense systems of insects, amphibians and mammals.[1, 2] Cecropin A, the first reported peptide of this type, is found in the *Cecropia* moth[3] and consists of 37 amino acid residues. Its antibacterial activity has been related to its ability to promote cell membrane lysis,[4, 5] although the detailed mechanism for this action is unclear. Melittin,[6] a 26-residue peptide that is the main component of the honey-bee venom, also has antibacterial properties, but is toxic to eukaryotic cells. Both cecropin A and melittin have been the object of structural studies attempting to understand their mode of action.[7–13] Different authors have investigated the effect of positive charge,[14, 15] net charge,[16] ionic strength,[17, 18] pH,[19] solvents, peptide concentration or side-chain length[10] in the structure of the peptides, both of which are known to adopt an α-helical conformation in the presence of organic solvents[11, 12] or micelles.[13, 14] Melittin forms aggregated structures (dimers, tetramers) under a variety of experimental conditions in solution, and crystallizes as a tetramer. This tendency to self-association is related to the highly amphipathic nature of its α-helical conformation.

In the course of studies aimed at finding peptides with improved antibacterial activity, a 15-amino acid hybrid peptide consisting of residues 1–7 of cecropin A followed by residues 2–9 of melittin (CA(1–7)M(2–9), Table 1) was found to retain the ability to adopt an amphipathic α-helical conformation and to display a broad and potent antibacterial spectrum and no cytotoxic character.[15, 16] The investigation of its conformational behaviour in solution under different experimental conditions should thus be helpful in identifying key structural features that determine the favourable biological properties of this peptide and should give insight for the design of even more active antibiotic peptides.

Previous CD and NMR work by our group and others[17, 18] had established that cecropin A–melittin hybrids were α-helical in the presence of hexafluoroisopropanol (HFIP) or of liposomes based on dimiristoyl phosphatidyl choline (DMPC).

[*] Miquel Pons, Imma Fernández, Josep Ubach, Monika Fuxreiter,[+] David Andreu
Departament de Química Orgànica, Universitat de Barcelona
Martí i Franquès 1-11, E-08028 Barcelona (Spain)
Fax: Int. code +(343)339-7878
e-mail: miquel@guille.qo.ub.es
José Manuel Andreu
CIB-CSIC, Velázquez 144, E-28006 Madrid (Spain)
[+] Present address: Eötvös Loránd University, Budapest (Hungary)

Table 1. Sequences of cecropin A, melittin and the hybrid peptide CA(1–7)M(2–9).

Peptide	Sequence
cecropin A	H–KWKLFKKIEKVGQNIRDGIIKAGPAVAVVGQATQIAKK–NH_2
melittin	H–GIGAVLKVLTTGLPALISSWIKRKRQQ–NH_2
CA(1–7)M(2–9)	H–KWKLFKKIGAVLKVL–NH_2

0947-6539/96/0207-0838 $ 15.00+.25/0

However, this tendency to adopt an α-helical structure could not be solely responsible for the membrane activity of CA(1–7)M(2–9), since its persuccinyl derivative had an even higher α-helical content in HFIP but no effect on the permeability of neutral liposomes.[17] Our own preliminary observations[17] have demonstrated that these peptides show a strong tendency to aggregate in solution, a property probably inherited from melittin and which we hypothesized might be relevant to the membrane activity of this peptide. In fact, while quaternary structure is rarely seen in small hydrophilic peptides, self-association is often found in membrane-active peptides.

In this paper we evaluate the extent and molecular determinants of self-association in CA(1–7)M(2–9) using a combination of physical methods (mass spectrometry, ultracentrifugation analysis, CD and NMR) and molecular modelling. The combined use of a variety of techniques provides enough constraints to characterize the self-association of CA(1–7)M(2–9). We suggest that self-association of cecropin A–melittin hybrids may enhance their biological activity by stabilizing the helical structure, favouring its binding to the membrane, and/or by helping to disrupt its structure.

Experimental Section

Abbreviations: CD, circular dichroism; COSY, correlation spectroscopy; DQF, double quantum filtered; ES-MS, electrospray ionization mass spectrometry; HFIP, hexafluoroisopropanol; NOE, nuclear Overhauser effect; NOESY, nuclear Overhauser effect spectroscopy; TFE, trifluoroethanol; TOCSY, total correlation spectroscopy.

Peptide Synthesis: The peptide CA(1–7)M(2–9) with the sequence shown in Table 1, was synthesized by solid-phase techniques and characterized as previously described.[16]

Circular Dichroism: CD spectra were recorded on a Jasco-720 spectropolarimeter. Cells with a path length of 0.5 to 0.02 cm were employed depending on peptide concentration. Temperature was maintained at 15 °C with a circulating water bath . Standard conditions were 25 μM peptide in either 5 mM phosphate buffer, pH 7.4, or 12% HFIP by vol. in water, pH 2.8. In different experiments peptide concentration was varied from 25 μM to 2 mM; HFIP concentration from 0 to 20% by vol.; phosphate concentration from 1 mM to 7 mM, and pH from 2.8 to 7.4. Spectra were recorded in a single scan using a bandwidth of 1 nm, 1 s time constant and a scan speed of 5 nm min^{-1}. Following baseline correction, the observed ellipticity was converted to mean residue ellipticity $[\theta]$ (deg cm^2 dmol^{-1}). The reference ellipticity for a 100% helical peptide of 15 residues is -33.000 deg cm^2 dmol^{-1} at 222 nm [19].

Ultracentrifugation: CA(1–7)M(2–9) was dissolved in 5 mM sodium phosphate buffer (pH 7.5), its partial specific volume (0.828 mL g^{-1}) was calculated and their molecular weights determined according to the expressions given by Laue et al. (1992) [20]. Samples containing 12% HFIP were prepared by adding the appropriate amount of this solvent to a solution of the peptide in 5 mM phosphate buffer. The pH of these samples was 6.5. Sedimentation equilibrium measurements were performed in a Beckman XLA analytical ultracentrifuge, employing sample volumes of 80 μL in two-channel and six-channel cells, in a titanium rotor at 40000 rpm and 25 °C. Radial scans of absorbance at 220, 280 and 300 or 310 nm were taken at 1 h intervals after 4 h centrifugation until equilibrium was achieved (successive scans give no signficant difference). Data were analysed with the programs Xlaeq, Eqassoc and the Origin Single and Multi self-association programs supplied by Beckman.

Mass Spectrometric Studies: Measurements were performed on a double quadrupole ion spray instrument (VG Quattro, Fisons Instruments, Altrinchman, UK) with a maximum range of 4000 *m/z*. The analysis conditions were: mobile phase 50% H_2O/50% ACN/1% formic acid, at a flow rate of 7 μL min^{-1}; an injection loop volume of 10 μL; nitrogen drying and nebulizing flow rates of 350 L h^{-1} and 10 L h^{-1}, respectively; capillary voltage 3.5 kV; a source temperature of 80 °C and a declustering potential of 45 V. Lyophilized samples of the peptide were dissolved with the necessary amount of water or water/hexafluoro-2-propanol containing 3% HCOOH to reach the desired concentrations of 500 and 100 μM.

NMR Spectroscopy: Assignments were carried out in spectra obtained at 500 MHz using a Varian VXR-500 spectrometer at a peptide concentration of 3 mM in either 85% H_2O/15% D_2O or in 73% H_2O/15% D_2O/12% [D_2]HFIP. pH (electrode reading) was 4.4 ± 0.1. Temperature was set to 5 or 30 °C, respectively. Dioxane was used as internal reference.

2D experiments included DQF-COSY, TOCSY with a mixing time of 80 ms, and NOESY with mixing times ranging from 100 to 400 ms. All NOE interactions were tested for spin-diffusion by analyzing the NOE build-up at different mixing times. Presaturation was used to suppress water in all the experiments. All two-dimensional data matrices (512 blocks of 35 scans) were zero-filled in both dimensions to obtain 4096 × 2048 time-domain data points and were subjected to gaussian apodization in both dimensions prior to Fourier transformation. Processing and analysis of the spectra was carried out using Varian VNMR software. Estimates of scalar ^3J(HN–Hα) coupling constants were obtained from DQF-COSY spectra. Proton–deuterium exchange in amide groups was measured at 25 °C on samples of CA(1–7)M(2–9) lyophilized from H_2O and dissolved in 12% [D_2]HFIP/88% D_2O, pH 3.0. One-dimensional spectra were acquired every 2 min over the first 4 h. Temperature coefficients were measured between 5 and 30 °C using TOCSY experiments in aqueous solution and from 1D experiments in 12% [D_2]HFIP.

Structure Calculations: 3D structures consistent with the experimental data were generated using a combination of distance-geometry (DGII program) with simulated annealing (Discover program) calculations. Both programs are implemented in the NMR Chitect package comercially available from Biosym.

NOE intensities were classified in three groups (weak, medium, strong) by estimating the intensities of the cross-peaks in the spectrum and correspond to upper-bound interproton distance restraints of 2.5, 3.5 and 4 Å, respectively. A set of 46 distance constraints derived from 17 sequential, 10 medium and long-range, and 19 intraresidual NOEs were used in the calculation of 10 simulated annealing structures derived from the best structures initially obtained by distance geometry. No H bond or dihedral constraints were used in the calculations starting from a monomeric structure. All simulated annealing runs produced structures that did not satisfy the experimental constraints well and consistently presented violations greater than 1.5 Å in three long-range NOEs.

A dimeric model was constructed by packing two antiparallel helices and assigning the three previously violated long-range NOEs (NH Leu4–Hα Ala10; NH Lys6–Hβ Val11 and Hβ Ile8–NH Lys13) as intermolecular. The database for each dimer contained 89 constraints. This model was submitted to distance geometry and simulated annealing, and produced dimeric structures that satisfied the experimental constraints well and did not present violations greater than 0.25 Å.

The simulated annealing protocol consisted of 100 steepest descent and 500 conjugate gradients minimization cycles, followed by 30 ps dynamics in which the temperature was raised from 0 to 1000 K, and the force constant on experimental NOE restraints was simultaneously increased. During the next 10 ps of dynamics at 1000 K the nonbond force constants were progressively raised to their value, and for the final 10 ps of dynamics the system was cooled to 0 K. The final structure was minimized using 1000 steepest descent and 1500 conjugate gradients cycles.

Molecular Modelling Calculations: Energy minimization and molecular dynamics simulations were carried out using Discover (CVFF force field). Calculations of the isolated peptide were started from an ideal α-helix generated by Insight II. The initial structures were first minimized using steepest descent followed by conjugate gradient algorithms. Periodic boundary conditions were applied to solvate the peptide. A cell of 2 × 34 × 25 Å^3 was used, filled with either 693 water or 159 octanol molecules. The cut-off was set to 12 Å. A number of aggregated structures was constructed using different symmetry operations. The size and tightness of the aggregates were determined in each case by the size of the cell. A melittin-like aggregate was constructed from the crystal structure of melittin [21] by keeping only residues 2–9 and appending at their N-terminus the sequence of residues 1–7 of cecropin A in an α-helical conformation. Periodic conditions were introduced using a cell defined with the parameters a = 61 Å, b = 38 Å, c = 42 Å, $\alpha = \beta = \gamma = 90°$, and the cut-off was set to 22 Å. The aggregates were extensively minimized before carrying out dynamic simulations.

Molecular dynamics simulations were carried out at 750 K (without solvent) or at 350 K (in aqueous and octanol solutions). After every 20 ps of dynamics, new velocities from Maxwellian distribution were given to all atoms of the last minimized structure and the whole process was reinitiated. Dynamics were analysed checking the preservation of an amount of helical structure compatible with the experimental observations. Simulations lasted 220 ps (in vacuo), 125 ps (water), 95 ps (octanol), and 50–250 ps in the aggregates.

Results

Circular Dichroism: CA(1–7)M(2–9) in water (pH 7.5) or in phosphate buffer (pH 6.8) shows a spectrum typical of a disordered peptide, with a minimum below 200 nm. In the presence of increasing amounts of HFIP a CD spectrum with two minima at 208 and 222 nm, typical of an α-helix, is observed. The conformational transition occurs between 12 and 14% HFIP in water solution (Fig. 1a) or between 4 and 8% HFIP in phosphate buffer (Fig. 1b). No isodichroic points are observed.[22]

  0947-6539/96/0207-0839 $ 15.00+.25/0

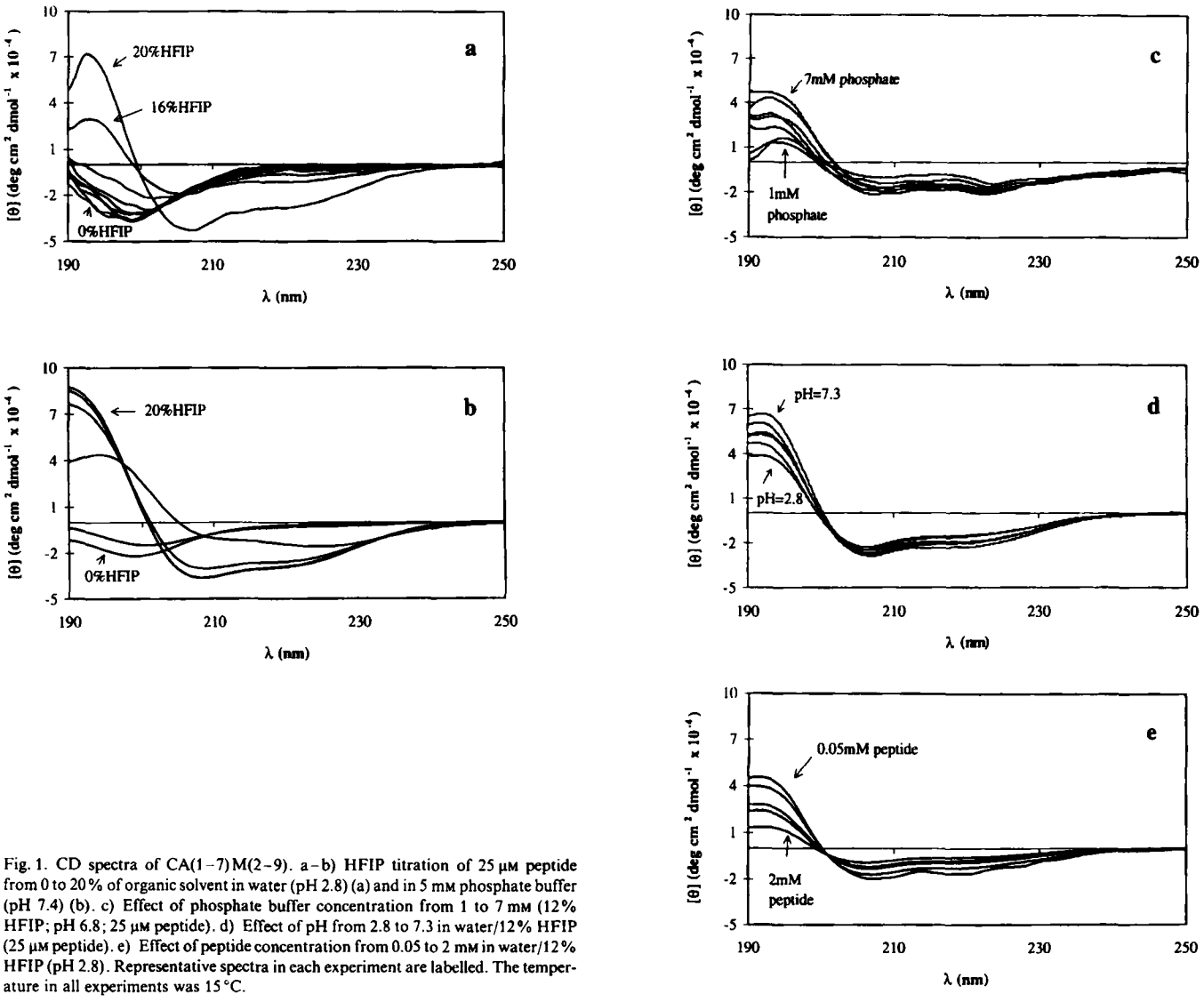

Fig. 1. CD spectra of CA(1–7)M(2–9). a–b) HFIP titration of 25 μM peptide from 0 to 20% of organic solvent in water (pH 2.8) (a) and in 5 mM phosphate buffer (pH 7.4) (b). c) Effect of phosphate buffer concentration from 1 to 7 mM (12% HFIP; pH 6.8; 25 μM peptide). d) Effect of pH from 2.8 to 7.3 in water/12% HFIP (25 μM peptide). e) Effect of peptide concentration from 0.05 to 2 mM in water/12% HFIP (pH 2.8). Representative spectra in each experiment are labelled. The temperature in all experiments was 15 °C.

At constant HFIP concentration the CD spectra of CA(1–7)M(2–9) depend on the concentration and pH of the buffer as well as on the peptide concentration, as discussed in the rest of this section.

CD spectra at different phosphate concentrations in 12% HFIP (pH 6.8) are shown in Figure 1c. The ellipticity between 205 and 230 nm decreases in absolute value with increasing phosphate concentration, and no isodichroic points are observed. In contrast, at pH 2.8 phosphate concentration has nearly no effect on the CD spectra of the peptide (data not shown). The CD spectra are pH-dependent with the negative ellipticity above 204 nm increasing with pH (Fig. 1d).

Figure 1e shows the CD spectra of CA(1–7)M(2–9) at different peptide concentrations in water containing 12% HFIP. In H_2O/HFIP solution the negative ellipticity above 200 nm decreases monotonically with concentration, and an apparent isodichroic point is observed at 200.6 nm. From 0.05 to 2 mM there is a 50% reduction in the ellipticity at 222 nm. In the presence of phosphate buffer (data not shown) there is also a general decrease in ellipticity at 208 and 222 nm, but the process seems to be far more complex, as seen by the absence of a proper isodichroic point and the non-monotonical decrease of ellipticity with concentration.

Ultracentrifugation: Sedimentation equilibrium analysis of a 450 μM solution of the peptide in phosphate buffer (Fig. 2a) gave a molecular weight of 1950 ± 270. Decreasing the concentration to 45 μM did not give significantly different results. Global fitting of the two sets of data gave no indication of

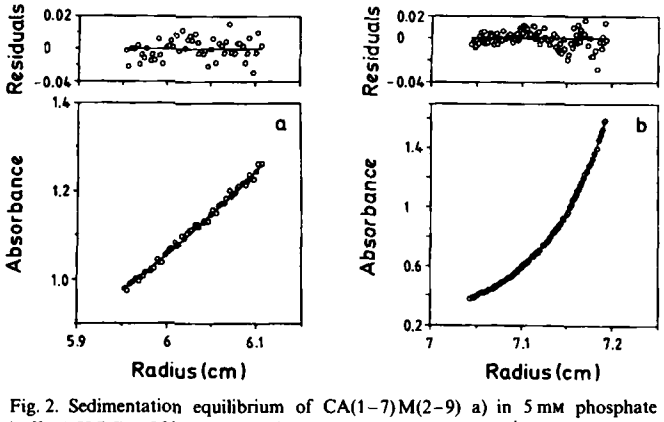

Fig. 2. Sedimentation equilibrium of CA(1–7)M(2–9) a) in 5 mM phosphate buffer (pH 7.5) at 25 °C and a peptide concentration of 4.5×10^{-4} M and b) in 5 mM phosphate buffer with 12% of HFIP (pH 6.5) at 25 °C and a peptide concentration of 4.2×10^{-4} M.

0947-6539/96/0207-0840 $ 15.00+.25/0 Chem. Eur. J. 1996, 2, No. 7

self-association and a molecular weight of 1760 ± 120 (allowing for non-zero baseline fitting). These results show that the peptide is essentially monomeric under these conditions. In small peptides such as this one, with a large number of charged groups, a certain overestimation of molecular weight may result from the effect of electrostriction on the partial specific volume, which is not taken into account in the standard calculation.[23, 24]

When 420 μM CA(1–7)M(2–9) was examined in 5 mM sodium phosphate/12% HFIP, at a pH of 6.5 and a temperature of 25 °C, the result was dramatically different from that in aqueous solution, and a much steeper concentration gradient was observed (compare Fig. 2a with 2b). In the absence of values for effective partial specific volume (ϕ) of peptides in this solvent (12% HFIP, density $\rho = 1.08\ g mL^{-1}$) only the buoyant effective molecular weight $M_b = M_r(1 - \phi\rho)$ could be measured with a value of 2510 ± 40. Global fitting of sedimentation equilibrium measurements at 420, 100 and 19 μM peptide gave no significant concentration dependence and an M_b value of 2840 ± 30.

ES-MS: There are several recent examples in the literature that illustrate the possibility of observing noncovalent interactions in biomolecules by means of mild-ionization mass spectrometric techniques (ion spray and electrospray).[25–27] ES-MS spectra of CA(1–7)M(2–9) (Fig. 3) contain the base peak at $m/z = 886$. This corresponds to the $2H^+$ charge state of the

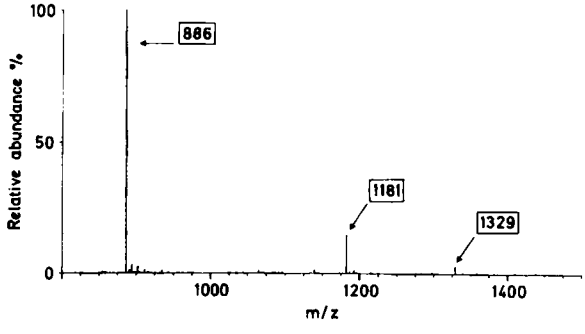

Fig. 3. ES-MS spectrum of 500 μM CA(1–7)M(2–9) dissolved in H_2O/HFIP (80:20) containing 3% formic acid.

monomer, although it could also contain contributions from oligomers having two charges per monomer. The less intense ions observed at an m/z of 1181 and 1329 can only be explained in terms of noncovalent association of the peptide. Under the same conditions, a very similar peptide (CA(1–7)M(3–10), H–KWKLFKKGAVLKVLT–NH_2), which showed no indications of aggregation by CD or NMR and which is not biologically active,[16] did not give peaks that could be attributed to multimeric species by ES-MS.

It is important in these studies to demonstrate that the high molecular weight species observed really reflect the presence of multimeric species in solution. We have studied the effect of peptide concentration and the addition of HFIP (20% in H_2O) on the corresponding ES-MS spectra. Table 2 shows the changes in relative abundance of the peaks of higher m/z values under the different conditions tested. The relative abundance of multimeric ions increases when the concentration is raised from 100 to 500 μM in the two sets of experiments. In addition, in the presence of HFIP these values are significantly higher than in pure water. The influence of the solvents on the intensities of the peaks corresponding to multimeric species indicates that the aggregated species are indeed present in solution and are not ionization artifacts.

Table 2. Relative abundance (r) of the peaks observed by ES-MS.

m/z	r/% [a] in H_2O [b]		r/% [a] in 20% HFIP/H_2O [b]	
	100 μM peptide	500 μM peptide	100 μM peptide	500 μM peptide
1181	3.36	9.55	13.79	14.38
1329	0.94	1.17	1.73	2.88

[a] Refers to the base peak at $m/z = 886$. [b] 3% HCOOH added.

Nuclear Magnetic Resonance: Standard NMR methods[28] were used to carry out a complete sequential assignment of ^1H NMR spectra of CA(1–7)M(2–9) in 15% D_2O/85% H_2O or in 15% D_2O/12% [D_2]HFIP/73% H_2O. NH–CHα cross-peaks were identified by DQF-COSY, and TOCSY spectra were used to correlate side-chain spin systems. NOESY cross-peaks correlating sequentially adjacent residues were used to obtain interresidue connectivities and to distinguish equivalent spin systems. Chemical shifts for all the protons in both solvents are reported in Table 3 . No significant changes in chemical shift were observed in TOCSY spectra recorded at peptide concentration from 0.5 to 6 mM in 12% HFIP or when the HFIP percentage was raised to 50% by volume.

Table 3. Chemical shifts of CA(1–7)M(2–9) at 30 °C and pH 4.4.

Residue	NH	Hα	Hβ	Others
K1	n.o.	4.01	1.89	γ: 1.45; δ: 1.69; ε: 2.98
W2	7.40	4.43	3.23; 3.15	2H: 7.24; 4H: 7.65; 5H: 7.17; 6H: 7.24; 7H: 7.50; NH: 10.22
K3	7.86	4.12	1.91	γ: 1.50; δ: 1.75; ε: 3.00
L4	7.22	4.12	189	γ: 1.89; δ: 0.92; δ′: 0.85
F5	7.70	4.14	3.70	2,6H: 7.10; 7,5H: 7.34; 4H: 7.25
K6	8.20	4.21	1.99	γ: 1.46; δ: 1.73; ε: 2.94
K7	7.62	4.20	1.73	γ: 1.58; δ: 1.46; ε: 3.04
I8	7.83	3.89	1.88	γ-CH_2: 1.61; γ′-CH_2: 1.25; γ-CH_3: 0.98; δ: 0.98; δ′: 0.89
G9	8.02	3.79		
A10	7.58	4.18	1.56	
V11	7.75	3.70	2.30	γ: 0.98; γ′: 1.08
L12	8.24	4.08	1.91	γ: 1.91; δ: 0.90
K13	7.80	4.13	2.05	γ: 1.43; δ: 1.75; ε: 3.02
V14	7.85	3.90	2.27	γ: 0.99; γ′: 1.11
L15	8.21	4.21	1.84	γ: 1.84; δ: 0.89

Differences between Hα and NH chemical shifts of CA(1–7)M(2–9) measured in 12% HFIP solution and in H_2O are shown in Figure 4. The upfield shifts induced in both Hα and NH protons by the addition of HFIP are consistent with the adoption of an α-helical conformation, mainly in the central region of the sequence.

The helical conformation was supported by the observation of strong NH_i–NH_{i+1} NOE together with weaker $H\alpha_i$–NH_{i+3} connectivities; these suggested the presence of a helical structure throughout most of the sequence (Fig. 4). An expansion of the NH–NH region of the NOESY spectra is shown in Figure 5. The lower intensity of NH–NH cross-peaks involving protons near the N-terminal region (e.g., Trp 2–Lys 3, or Lys 3–Leu 4) as well as the smaller upfield shifts in this region suggested some helical fraying in this terminal region. In contrast, the helical structure appeared well formed up to the last residue in the C-terminus. Additional long-range NOEs were observed between HαLys 3–NH Lys 7, NH Leu 4–Hα Ala 10, NH Lys 6–Hβ Val 11 and Hβ Ile 8–NH Lys 13. NOE build-up curves involving these signals are comparable to those for other NOE

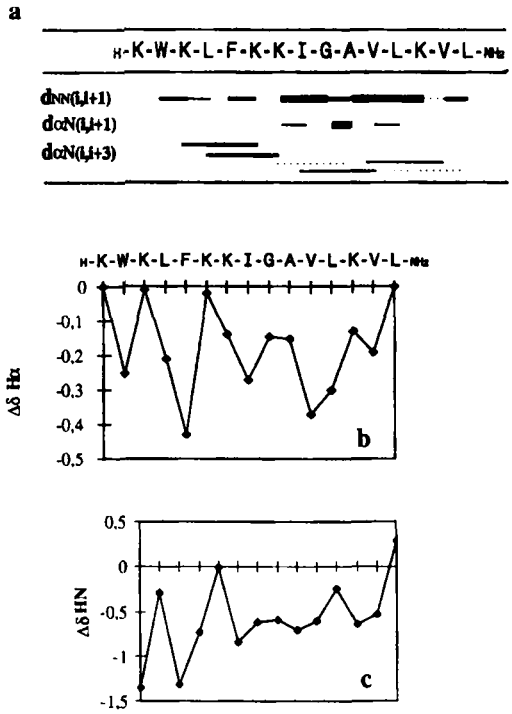

Fig. 4. a) Summary of sequential and medium-range NOEs of 3 mM CA(1–7)M(2–9) in 12% [D$_2$]HFIP at 30 °C (pH 4.4). b–c) Conformational shifts of Hα and NH protons, respectively, under the same conditions as indicated in a).

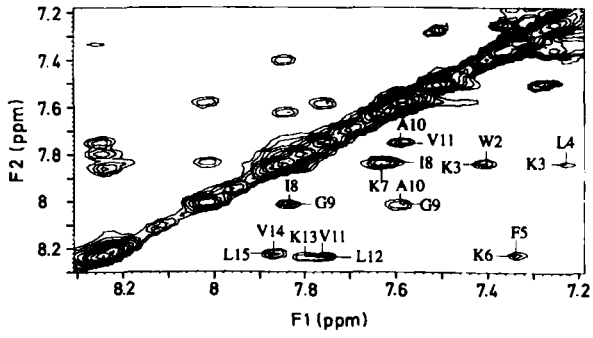

Fig. 5. Sequential NH–NH cross-peak region of a 400 ms NOESY of 3 mM CA(1–7)M(2–9) in 73% H_2O/15% D_2O/12% [D$_2$]HFIP (pH 4.4, 30 °C).

cross-peaks; this indicates that they correspond to short distances and are not caused by spin-diffusion.

In spite of the small size of CA(1–7)M(2–9), several amide protons were found to exchange very slowly with deuterium in the presence of 12% [D$_2$]HFIP. Figure 6 shows the decay of

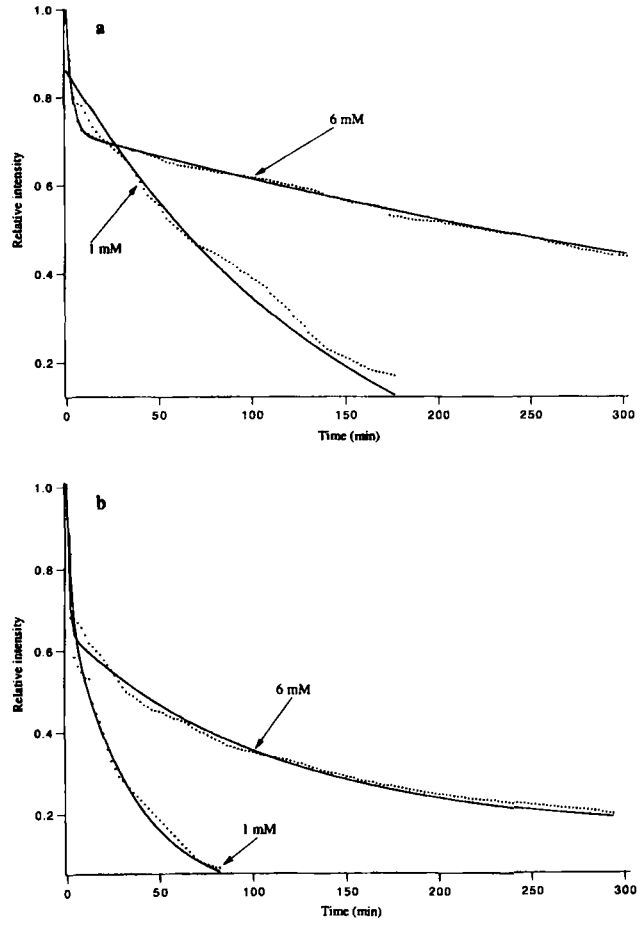

Fig. 6. Plot of the residual intensity of the amide protons of Leu12 (a) and Val14 (b) at different times after dissolving CA(1–7)M(2–9) in 88% D_2O/12% [D$_2$]HFIP at a concentration of 1 or 6 mM. Continous lines represent the best fits to a biexponential curve.

amide proton occupancy in residues Leu12 (Fig. 6a) and Val14 (Fig. 6b) of CA(1–7)M(2–9) at two concentrations. These curves do not follow a single exponential. The simplest model to which the experimental data could be fitted is a biexponential decay, suggesting the existence of peptide molecules in at least two different environments. The amplitudes and rate constants are presented in Table 4. The lower exchange rate is strongly concentration-dependent; this indicates that protection from exchange is a result of the quaternary structure of the peptide. The different environments could result either from different degrees of aggregation in solution or from nonequivalent environments within an aggregate.

Table 4. HD Exchange rates of CA(1–7)M(2–9) amide protons [a].

Residue	1 mM concentration				6 mM concentration			
	f_1 [b]	$k_1 \times 10^4$ (s^{-1})	f_2 [b]	$k_2 \times 10^4$ (s^{-1})	f_1 [b]	$k_1 \times 10^4$ (s^{-1})	f_2 [b]	$k_2 \times 10^4$ (s^{-1})
Phe5			1.00	12.4			1.00	7
Ile8	0.53	2	0.47	50	0.85	0.7	0.15	5
Gly9	–	–	–	–	0.70	0.8	0.30	60
Ala10 [c]	–	–	–	–	–	–	–	–
Val11	0.61	2	0.39	60	0.67	0.5	0.33	1.3
Leu12	0.85	0.8	0.15	50	0.69	0.3	0.31	50
Lys13	–	–	–	–	0.74	1	0.26	70
Val14	0.66	4	0.34	70	0.58	2	0.42	14

[a] Measured in 12% [D$_2$]HFIP at pH = 3.4 (electrode reading) and 25 °C. [b] f_1 and f_2 refer to the relative contribution of the slow (rate k_1) and fast (rate k_2) component to the observed decay. [c] Overlaps with an aromatic proton.

0947-6539/96/0207-0842 $ 15.00+.25/0 Chem. Eur. J. 1996, 2, No. 7

Discussion

α-Helical conformation and aggregation: The antibiotic activity of cecropin–melittin hybrids has been correlated with their ability to adopt an α-helical structure in helix-inducing solvents such as HFIP or in the presence of liposomes. The intrinsic propensity of the sequences involved towards forming helices, however, is very low, and when calculated[29] in a series of variants of CA(1–7)M(2–9), it does not correlate with the measured helical content or the biological activity. On the other hand, the amphipathic nature of the helix suggests that intermolecular contacts are an essential part of the stabilizing interactions of the helical structure.

Formation of an α-helix by CA(1–7)M(2–9) can be followed by CD and NMR under different experimental conditions. Addition of HFIP (or liposomes[17]) is essential to induce an α-helical conformation; however, the amount of helix detected by CD is also dependent on pH, phosphate concentration and peptide concentration, with a complex interplay between all these variables.

An increase in pH promotes the helical conformation probably by deprotonation of the N-terminal amino group resulting in a decrease in the electrostatic repulsion with the positive end of the helix macrodipole.

An increase in phosphate buffer concentration, at a constant pH of 6.8 and a peptide concentration of 25 μM, causes an apparent reduction of the helix content, but has no effect when the pH is kept constant at 2.8. This suggests that the interaction with phosphate can raise the apparent pK_a, and thus increase the degree of ionization of the N-terminal amino group, which destabilizes the helix. Furthermore, the increase in ionic strength should reduce the electrostatic repulsion between the highly charged peptide molecules and promote aggregation. Similar phenomena have been observed in melittin.[8]

Concentration-dependent CD spectra are indeed indicative of aggregation phenomena in CA(1–7)M(2–9). Both in the presence and absence of phosphate buffer, an increase in peptide concentration leads to a *decrease* in the ellipticity at 222 nm. In phosphate-free solution, of pH 2.8 and containing 12% HFIP, an apparent isodichroic point suggests that the concentration-dependent CD contribution behaves as a two-state equilibrium, while a much more complex behaviour must be taking place in phosphate buffer/12% HFIP.

The decrease in ellipticity at 222 nm with increased peptide concentration contrasts with the usual behaviour of peptides capable of adopting an amphipathic α-helical structure. The usual observation is that self-association of the peptide stabilizes the α-helix, and therefore at higher concentrations the ellipticity at 222 nm, usually taken as a direct measure of the helix content, increases in absolute value.

The amount of helical structure can be quantified independently by NMR by comparing the chemical shifts with reference values for a disordered peptide.[30, 31] Chemical shifts can be measured accurately at lower concentrations than any other conformationally sensitive NMR parameter. Ideally, these values should be measured in the same peptide under denaturing conditions. CD spectra indicate that CA(1–7)M(2–9) is basically disordered in H_2O, and the chemical shift values measured in this solvent were therefore used. Moreover, it has been reported that, if no conformational change takes place, chemical shifts are not very sensitive to changes from water to 30% TFE, a solvent very similar to HFIP.[32] An average conformational shift was calculated by adding all Hα upfield shifts (lacking stereospecific assignment, we used the larger upfield shift of Gly) and dividing by the total number of peptide bonds. To obtain the overall helical contents we divided the average conformational shift by 0.35 ppm, which was taken as an average for 100% helicity.[33] This calculation indicates a 52% helix for CA(1–7)M(2–9) in 12% HFIP. Chemical shifts are independent of concentration in the range from 0.5 to 6 mM and, therefore, the helix content calculated from NMR is also constant in this concentration range. The helix content derived from NMR is in good agreement with that calculated by CD in the same solvent, but at a concentration of 0.05 mM (52%).

The apparent loss of helicity observed in the CD spectra at higher concentrations is not confirmed by the NMR data. Distortions in the absorption and CD spectra of aggregating peptides have been reported for polyglutamic acid[34] and attributed to Duysens absorption flattening and scattering. Both phenomena are in fact related in the Mie scattering theory.[35] These effects are important when the particle size becomes comparable to the wavelength and therefore would imply the formation of large aggregates (more than 10 monomers) of CA(1–7)M(2–9) in the helical form. Aromatic side-chain contributions to far-UV CD spectra have been reported to cause significant errors in the calculation of helical content from ellipticity measurements at 222 nm.[36] In non-aggregating peptides a Trp residue causes an overestimation of the helicity, while Tyr causes up to a 20% underestimation. This effect has been attributed to a reduction in flexibility of the aromatic ring in the helical peptide. The effect observed when the concentration of tryptophan-containing CA(1–7)M(2–9) is increased is opposite in sign (apparent helicity is reduced) and stronger than that observed by Chakrabarthy et al.[36] It is reasonable that aggregation could also restrict the mobility of Trp, but induce an orientation different than that caused by simple helix formation. Therefore, the contribution of the aromatic side-chain to the apparent reduction of helicity upon aggregation cannot be ruled out.

Further evidence for the presence of aggregated species in HFIP containing solutions comes from ultracentrifugation and ES-MS studies.

The molecular weight calculated in phosphate buffer (1760 ± 120) is in good agreement with the expected value for a monomeric peptide (1770) and does not change with concentration. In the same buffer, with 12% HFIP, a completely different concentration gradient is established. However, no significant differences were observed when the initial concentration was varied from 19 to 0.42 mM.[37] The value of the buoyant effective molecular weight M_b of 2840 ± 30 indicates that CA(1–7)M(2–9) undergoes significant self-association in this solvent at all the concentrations studied, since otherwise negative or unreasonably low partial specific volumes would be required to satisfy the equation $M_b = M_r(1 - \phi\rho)$. The degree of aggregation is probably large, in the order of 10 monomers.[38] These results, along with the CD data presented above, demonstrate that a helical conformation is required for aggregation and that large aggregates are formed.

Peaks at an m/z of 1181 and 1329 in the ES-MS spectra of CA(1–7)M(2–9) have been assigned to multimeric species on the basis of the increase in intensity observed at higher concentration. These peaks also increase in intensity on addition of HFIP, in agreement with CD and ultracentrifugation studies, which indicate substantial aggregation in solution in the presence of HFIP.

Formation of the multiply charged species causes an uncertainty as to the actual molecular weight of the observed species. The smallest aggregate that could explain simultaneously all the observed peaks is a hexamer, but the possibility that several aggregated species are simultaneously present cannot be ruled

out. The smallest aggregates that would explain the more intense peaks at m/z 1181 and 1329 are a dimer ($3H^+$) and a trimer ($4H^+$), respectively.[39] Ultracentrifugation studies suggest, however, a degree of aggregation higher than ten, and deuterium exchange experiments (see below) provide an estimation of six peptides in the aggregated form.

Structure of the aggregates: NMR studies can provide information on the structure of the aggregate formed by CA(1–7)M(2–9). Conformational shifts and NOE results in the presence of HFIP indicate an α-helical structure spanning most of the peptide, although with some fraying in the N-terminal part. The residues showing extreme Hα or amide helix shifts align along interface boundaries and define what is known as hydrophobic period.[40] This helix shift periodicity is clearly shown in conformational shift profiles (Fig. 4), and the extreme negative values correspond to hydrophobic residues in the sequence (Leu4, Ile8, Val11 and Val14) and to aromatics, although the latter may be affected by ring-current shifts. This behaviour has been interpreted as the result of periodic distortions from regular helix geometry associated with intermolecular packing of helices.[40, 41]

Three long-range NOEs observed, namely, NH Leu4–Hα Ala10, NH Lys6–Hβ Val11 and Hβ Ile8–NH Lys13, are not compatible with a single α-helical structure. Two of the residues involved (Val11 and Ile8) have NH protons that are protected from exchange at 1 mM peptide concentration, and Lys13 is also protected at higher concentration. Therefore, it seems a reasonable assumption to assign these NOEs as intermolecular contacts in the aggregate. In a fully helical peptide, residues Leu4, Ile8 and Val11 would cluster in one side of the helix, while Ala10, Lys6 and Lys13 would form a similar pattern in the opposite side. Interestingly, the three NH protons involved in long-range contacts do not present NH_i–NH_{i+1} NOEs. This suggests that there is a local distortion of the helical structure; however, the observation of $CH\alpha_i$–NH_{i+3} NOEs spanning these points indicates that the overall helical structure is maintained.

Simulated annealing runs included the observed long-range NOEs as intermolecular constraints linking residues 4, 8 and 11 in one molecule to residues 6, 10 and 13 in a second molecule to produce a dimer in which the two monomers are packed in an antiparallel fashion. In this model, residues 6, 10 and 13 of the first molecule and residues 4, 8 and 11 of the second one are still available to interact with additional peptide molecules, thus allowing the build-up of the higher aggregates observed by ultracentrifugation or ES-MS.[42] A schematic drawing of this model of aggregate is shown in Figure 7.

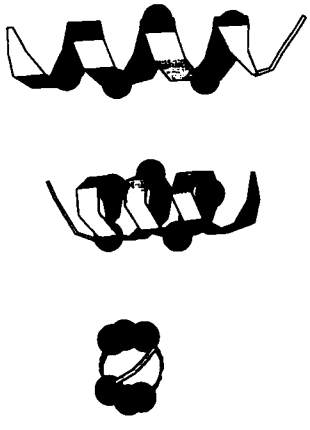

Fig. 7. Schematic MOLSCRIPT [49] representation of the packing of three ideal helices of CA(1–7)M(2–9) in an aggregate. The last three residues are represented by a thin ribbon to help visualize the antiparallel packing. Residues involved in intermolecular NOE contacts are highlighted. Interhelical distances have been increased for clarity.

Deuterium exchange experiments can provide additional information on the nature and stability of the aggregates formed by CA(1–7)M(2–9). As seen in Figure 6 and Table 3, a fast and a slowly exchanging component can be detected for most of the residues near the C-terminus of the peptide, and the rates of decay of the slowly decaying components are concentration dependent; this shows that aggregation effects are responsible for the observed slow exchange.

In the model of aggregation suggested by the NOE data, long chains of laterally packed α-helical peptides are formed. One could therefore assign the slowly exchanging component to peptide molecules located in the interior of the aggregate and the fast exchanging component to molecules situated at the end of the chain. Thus, the ratio between the fast and slow rate constants provides a measure of the extra protection of amide protons in the inner molecules.[43] Protection to deuterium exchange has been recently used to derive dimerization constants in glycopeptide antibiotics,[47] assuming that an EX2 mechanism is operative, that is, deuterium exchange is slow relative to the on-rate for dimerization. The concentration dependence of the rate of exchange suggests that this mechanism is also applicable for CA(1–7)M(2–9), although a complete treatment is complicated by the fact that higher order aggregates are involved. However, a simplified approach is possible as shown schematically in Figure 8. If a chain breaks, two inner molecules, which had slowly exchanging amide protons, will become terminal, and their amide protons will exchange faster. Conversely, the interacting ends of two chains that are joined together become protected. One can thus define a pseudodimerization constant (K_n) for the process of joining two chains of $n/2$ molecules to give an aggregate of n monomers [Eq. (1)]. In the simplest case, where microscopic constants describing the addition of a new molecule to the aggregate are independent of the size of the aggregate, this pseudodimerization constant would be numerically equivalent to the dimerization constant and therefore provides a measure of the stability of the aggregate. This constant can be determined from the ratio R between the slow and fast rate constants of exchange and the total peptide concentration (c_T), by using a staightforward modification of the method described by Mackay et. al [Eq. (2)].[47] In CA-(1–7)M(2–9) the protection factor (R^{-1}) has a maximum value of around 60 at 1 mM and ca. 170 at 6 mM for Leu12. Amide

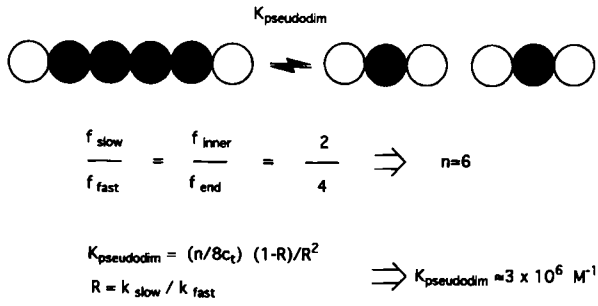

Fig. 8. Schematic representation of a linear aggregate of CA(1–7)M(2–9). Molecules with fast-exchanging amide protons are represented by open circles, and those contributing the slow-exchanging components are shown as filled circles. The average size of the aggregate can be obtained from the relative populations of the two components. An estimate of the apparent dimerization constant is provided by the relative rates of exchange of the two components.

$$2P_{n/2} \longrightarrow P_n \qquad K_n = \frac{[P_n]}{[P_{n/2}]^2} \tag{1}$$

$$K_n = -\frac{n}{8c_T}\frac{R-1}{R^2} \text{ with } R = \frac{k_{slow}}{k_{fast}} \tag{2}$$

0947-6539/96/0207-0844 $ 15.00+.25/0 Chem. Eur. J. 1996, 2, No. 7

protons located either side in the sequence show lower protections. The pseudodimerization constant has a value of ca. $3 \times 10^6 \text{M}^{-1}$ ($n = 6$). If slow and fast exchanging components can be related to inner and terminal molecules in a linear aggregate, the relative populations of the two types of molecules provide an estimate of the length of the chain. The slow exchanging component represents ca. 60–70% of the total population. If the distribution of sizes were monodisperse, this would indicate a chain of six molecules (4/6 = 0.67), in agreement with the ES-MS and ultracentrifugation results, although other distributions, for example, involving the coexistence of shorter and longer chains, could explain the same results.

The structure of the dimer of CA(1–7)M(2–9) suggested by NMR exhibits the same antiparallel topology of melittin dimers found in crystallography. In order to test this idea, CA(1–7)M(2–9) dimers were modelled starting from a structure in which the last eight residues (i.e., those with the sequence of melittin (2–9)) were in the position found in the crystal structure of melittin dimers and the rest were constructed in an ideal α-helical conformation. The simplicity of the modelling compared to the complexity of the system studied allows only a qualitative analysis of the calculations, and we concentrated on the preservation or otherwise of the helical structure. After extensive minimization and 50 ps of dynamics under periodic boundary conditions that reproduced the periodicity present in the crystal, the final structure retained the helical conformation of the C-terminal part with some unfolding in the N-terminus and the same topology as that generated from the NMR information, although, not surprisingly, the structural details and in particular the observed long-range NOEs were not reproduced. In contrast, the same peptide solvated in water or in a number of aggregates built up using ideal α-helices interacting with equivalent images obtained by symmetry operations had lost completely the helical conformation after the first 20 ps of dynamics.

Conclusions

CA(1–7)M(2–9) has been found to adopt a helical conformation in the presence of HFIP or liposomes and to associate strongly in the presence of HFIP. Estimates of the association constant, stoichiometry and structure of the aggregates have been derived from CD, ultracentrifugation, ES-MS, NOE data and HD exchange. The relevance of aggregation for the biological activity of CA(1–7)M(2–9) remains to be established. Current research in our laboratory has demonstrated a correlation between antibiotic potency and tendency to aggregate in different related peptides.[48] However, as aggregation is also related to the amphipathicity of the sequence, this correlation does not necessarily imply a causal relationship between aggregation and biological activity. There are plenty of examples of amphipathic helices stabilized by dimerization. In this case helix formation and dimerization are coupled phenomena. On the other hand, binding to membranes has been shown to induce helicity in CA(1–7)M(2–9).[17] It is then possible that the three processes of membrane binding, formation of a helix and oligomerization are also coupled in CA(1–7)M(2–9). Aggregation of the helical peptide within the membrane could therefore result in an increase in the effective binding constant.

Acknowledgments: The provision of a predoctoral fellowship from the Ministerio de Educación y Ciencia (Spain) to I. F. and J. U. is gratefully acknowledged. M. F. held a Tempus Program Grant. We wish to thank Dr. German Rivas, from the "Centro de Investigaciones Biológicas del CSIC", for advice on analytical centrifugation. We acknowledge the use of the NMR and CD facilities of the "Serveis Científico-Tècnics" of the University of Barcelona. This work was supported by funds from DGICYT (PB94-924 and PTR93-0032) and Fondo de Investigaciones Sanitarias (94/0007/01).

Received: September 29, 1995 [F222]

[1] H. G. Boman, *Cell* **1991**, *65*, 205–207.
[2] H. G. Boman, D. Hultmark, *Ann. Rev. Microbiol.* **1987**, *41*, 103–126.
[3] H. Steiner, C. Hultmark, A. Engström, H. Bennich, H. G. Boman, *Nature* **1981**, *292*, 246–248.
[4] E. Habermann, *Science* **1972**, *177*, 314–322; 1683–1688.
[5] E. Habermann, H. Kowallek, *Hoppe-Seyler's Z. Physiol. Chem.* **1970**, *351*, 884–890.
[6] K. Ramaligan, S. Aimoto, J. Bello, *Biopolymers* **1992**, *32*, 981–992.
[7] Y. Hagihara, M. Kataoka, S. Aimoto, Y. Goto, *Biochemistry* **1992**, *31*, 11908–1114.
[8] L. R. Brown, J. Laiterwein, K. Wuthrich, *Biochim. Biophys. Acta* **1980**, *622*, 231–244.
[9] J. Bello, H. R. Bello, E. Granados, *Biochemistry* **1982**, *21*, 461–465.
[10] K. Ramaligan, J. Bello, *Biochemistry* **1993**, *32*, 253–259.
[11] T. A. Holak, A. Engström, P. J. Kraulius, G. Lindeberg, H. Bennich, T. A. Jones, A. M. Gronenborn, G. M. Clore, *Biochemistry* **1988**, *27*, 7620–7629.
[12] B. Bazzo, M. J. Tappin, A. Pastore, T. S. Harvey, J. A. Carver, I. D. Campbell, *Eur. J. Biochem.* **1988**, *173*, 139–146.
[13] H. Vogel, F. Jähnig, *Biophys. J.* **1986**, *50*, 573–582.
[14] H. S. Mchaourab, J. S. Hyde, J. B. Feix, *Biochemistry* **1994**, *33*, 6691–6699.
[15] D. Wade, D. Andreu, S. A. Mitchell, A. V. Silveira, I. A. Boman, H. G. Boman, R. B. Merrifield, *Int. J. Peptide Protein Res.* **1992**, *40*, 429–436.
[16] D. Andreu, J. Ubach, I. A. Boman, B. Wåhlin, D. Wade, R. B. Merrifield, *FEBS Lett.* **1992**, *296*, 190–194.
[17] I. Fernández, J. Ubach, F. Reig, D. Andreu, M. Pons, *Biopolymers* **1994**, *34*, 1251–1258.
[18] D. Sipos, K. Chandrasekhar, K. Arvidsson, A. Engström, A. Ehrenberg, *Eur. J. Biochem.* **1991**, *199*, 285–291.
[19] Y. H. Chen, J. T. Yang, K. H. Chan, *Biochemistry* **1974**, *13*, 3350–3359.
[20] T. M. Laue, D. S. Bhairavi, T. M. Ridgeway, S. L. Pelletier, in *Analytical Ultracentrifugation in Biochemistry and Polymer Science* (Eds.: S. E. Harding, A. J. Rowe, J. C. Horton), Royal Society of Chemistry **1992**, pp. 90–125.
[21] T. C. Terwilliger, D. Eisenberg, *J. Biol. Chem.* **1982**, *257*, 6016–6022.
[22] Although a true isodichroic point is expected only for a pure two-state transition, strongly cooperative helix-coil transitions offen give apparent isodichroic points. The pH dependency of the CD spectra of CA(1–7)M(2–9) adds to the complexity of the HFIP-induced transition, as HFIP is very acidic due to the effect of the six fluorine groups, and the pH of the solution varies by ca. one pH unit during the titration.
[23] M. A. Starovasnik, T. K. Blackwell, T. M. Laue, H. Weintraub, R. E. Klevit, *Biochemistry* **1992**, *31*, 9891–9903.
[24] C. P. Kharakoz, *Biophys. Chem.* **1989**, *34*, 115–125.
[25] M. Busman, D. Knapp, L. Schey, *Rapid Comm. Mass Spectrom.* **1994**, *8*, 211–216.
[26] Y. Li, Y. Hsieh, J. D. Henion, M. W. Senko, F. W. McLafferty, B. Ganem, *J. Am. Chem. Soc.* **1993**, *115*, 8409–8413.
[27] M. Baca, S. B. H. Kent, *J. Am. Chem. Soc.* **1992**, *114*, 3992–3993.
[28] K. Wüthrich, *NMR of Proteins and Nucleic Acids*, John Wiley, New York **1986**.
[29] V. Muñoz, L. Serrano, *Nature: Struct. Biol.* **1994**, *1*, 399–409.
[30] J. Nelson, N. Kallenbach, *Biochemistry* **1989**, *28*, 5256–5261.
[31] M. Bruix, M. Perello, J. Herranz, M. Rico, J. L. Nieto, *Biochem. Biophys. Res. Commun.* **1990**, *167*, 1009–1014.
[32] M. A. Jimenez, J. L. Nieto, J. Herranz, M. Rico, J. Santoro, *FEBS Lett.* **1987**, *221*, 320–324.
[33] J. Rizo, F. J. Blanco, B. Kobe, M. D. Bruch, L. Gierasch, *Biochemistry* **1993**, *32*, 4881–4894.
[34] D. W. Urry, T. A. Hinners, L. Masotti, *Arch. Biochem. Biophys* **1970**, *137*, 214–221.
[35] D. J. Gordon, *Biochemistry* **1972**, *11*, 413–420.
[36] A. Chakrabarty, T. Kortemme, S. Padmanabhan, R. L. Baldwin, *Biochemistry* **1993**, *32*, 5560–5565.
[37] The lack of concentration dependence of the ultracentrifugation data contrasts with the CD results, which show a considerable variation in the same concentration range. This may be due to the different sensitivities of the two techniques or to small differences in pH between samples, which could cause significant differences in the degree of aggregation, since the pH of 6.5 is very close to that at which the onset of precipitation in 5 mM phosphate and 12% HFIP occurs.
[38] Although the partial specific volume of the peptide in 12% HFIP is not known, assuming values in the range $0.828 \pm 0.050\ \text{mL g}^{-1}$ would give molecular weights in the interval $17500 < M_r < 52600$.
[39] Samples for ES-MS were unbuffered. As the presence of phosphate tends to increase the degree of aggregation, ES-MS results are expected to be more directly comparable to NMR results, which were also recorded in an unbuffered sample.

[40] F. J. Blanco, J. Herranz, C. González, M. A. Jiménez, M. Rico, J. Santoro, J. L. Nieto, *J. Am. Chem. Soc.* **1992**, *114*, 9676–9677.
[41] N. E. Zhou, B. Y. Zhu, B. D. Sykes, R. S. Hodges, *J. Am. Chem. Soc.* **1992**, *114*, 4320–4326.
[42] If the same packing is maintained between each adjacent molecule in the aggregate, the resulting particle would have the structure of a cholesteric liquid crystal and that might provide an additional explanation for the change in the intensity of the CD spectra of the aggregate as compared to the monomeric helix.
[43] Protection factors are usually calculated with reference to fully exposed NH protons. The presence of 12% HFIP is expected to shift the pH of minimum exchange to higher values [44], but the acidic character of the hydroxyl proton of HFIP could introduce a general acid catalytic effect. The presence of multiple positive charges in the peptide introduces a further complication as it tends to shift the pH_{min} to lower values [45] partially offsetting the effect of the organic solvent. The calculated rate for an exposed NH in poly-Ala in D_2O at pH 4.4 and 30 °C is ca. 3.3×10^{-2}, and there is a fourfold decrease in the rate for branched residues [46]. With this reference, even fast components would qualify as protected, in agreement with other NMR observations indicating that this region forms a helical structure.
[44] J. J. Englander, J. R. Rogero, W. Englander, *Anal. Biochem.* **1985**, *147*, 234–244.
[45] P. S. Kim, R. L. Baldwin, *Biochemistry* **1982**, *21*, 1–5.
[46] A. D. Roberston, R. L. Baldwin, *Biochemistry* **1991**, *30*, 9907–9914.
[47] J. P. Mackay, U. Gerhard, D. A. Beauregard, R. A. Maplestone, D. H. Williams, *J. Am. Chem. Soc.* **1994**, *116*, 4573–80.
[48] J. Ubach, I. Fernandez, D. Andreu, M. Pons, unpublished results.
[49] P. J. Kraulis, *J. Appl. Crystallogr.* **1991**, *24*, 946–50.

0947-6539/96/0207-0846 $ 15.00+.25/0